Puay, H. T.; Hosoda, T.

Fundamental Characteristics of Open Channel Flows near An Abrupt Expansion

Proceedings of ninth International Conference on Hydro-Science and Engineering (ICHE 2010), IIT Madras, Chennai, India.
2 - 5 August 2010

on

FUNDAMENTAL CHARACTERISTICS OF OPEN CHANNEL FLOWS NEAR AN ABRUPT EXPANSION

H.T. Puay[1] and T. Hosoda[2]

Abstract: *This paper deals with the study of free surface flow near an abrupt expansion in an open-channel. A three dimensional free-surface numerical model is developed to simulate the phenomenon. The numerical model is based on the Volume of Fluid (VOF) method. Cubic-Interpolated Propagation (CIP) scheme is used to solve the advection term in the Navier-Stokes equation as well as the advection of the VOF density function, F. The numerical results are verified using the analytical solutions derived using the method of characteristics. Both numerical and analytical results are compared with the laboratory experiment results.*

Keywords: *open-channel flow; free surface numerical model; VOF method; CIP schem; method of characteristic.*

INTRODUCTION

The abrupt expansion flow is a ubiquitous and important phenomenon in open-channel flow that deserves rigorous study. It occurs when flow is subjected to sudden or abrupt flow area change or transition due to the change in the geometry of the channel. The abrupt expansion flow phenomenon can be observed at the outlet of a channel discharging into a wider channel and also in the transition section of a spillway. The understanding of the attributes of the abrupt expansion flow phenomenon such as the flow expansion angle and the formation of show waves is vital for more efficient hydraulic structure design.

Studies have shown that the phenomenon of abrupt expansion flow depends on the channel approach width b, the approach flow depth h_0 and the approach Froude number, Fr (Ippen, 1951, Hager, 1992, Hosoda, 1994). The relation between Froude number and the change of flow direction for supercritical flow was derived by Ippen (1951) and Hosoda (1994) through different approach. In this study, a free-surface numerical model based on the VOF method is developed to simulate the abrupt expansion flow phenomenon. The advection term in the Navier-Stokes equation is solved using a higher order scheme, CIP. Instead of the donor-acceptor scheme in the original VOF method, the advection of VOF density function, F is also solved with CIP scheme. Analytical solution for the flow expansion angle (angle of change in flow direction), θ is derived based on a steady state depth averaged model using method of characteristics. Both analytical and numerical findings are compared with laboratory experimental results.

1 Phd Student, Department of Urban Management, Graduate School of Engineering, Kyoto University, C1-3, Kyoto Daigaku Katsura, 615-8540, Nishikyou-ku, Kyoto, Japan, Email: eddiepuay@gmail.com
2 Professor, Department of Urban Management, Graduate School of Engineering, Kyoto University, C1-3, Kyoto Daigaku Katsura, 615-8540, Nishikyou-ku, Kyoto, Japan, Email: hosoda@mbox.kudpc.kyoto-u.ac.jp

ABRUPT EXPANSION FLOW CHARACTERISTIC

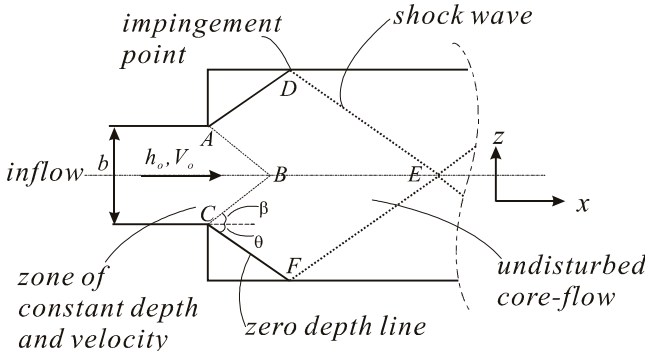

Fig. 1. Flow configuration of super-critical flow near the abrupt expansion.

The steady state abrupt expansion flow characteristics are shown in Figure 1 for super-critical flow. As the inflow passes through the section of abrupt expansion, the flow direction changes due to the abrupt change in the flow cross section area. However, there is a zone close to the abrupt expansion (zone ABC) where the flow velocity and depth are constant and equivalent to the approach flow depth h_o and velocity V_o. This triangular zone is known as the zone of constant depth and velocity (Hosoda, 1994). The flow impinges the channel wall at point D and F at an angle θ. The line AD and CF form the zero-depth line defining the boundary between the flow and the dry corner.

At impingement points F and D, the flow direction is again subjected to change as the channel wall aligns the flow direction. The flow is aligned parallel to the channel walls. Due to the change of flow direction after impingement at point F and D, shock waves are formed. These shock waves propagate towards the opposite channel walls, indicated by line DE and FE and will meet at point E before changing its directions again after point E. Since the channel wall reflects the flow direction inwards at impingement points F and D, the shock wave is a positive disturbance in the form of a surge wave that causes the rise in flow depth in the area between line DE and the boundary wall (and also area between line FE and the boundary wall). The zone ADEFC is therefore the core-flow where the flow is undisturbed by shock waves FE and DE (Hager, 1992).

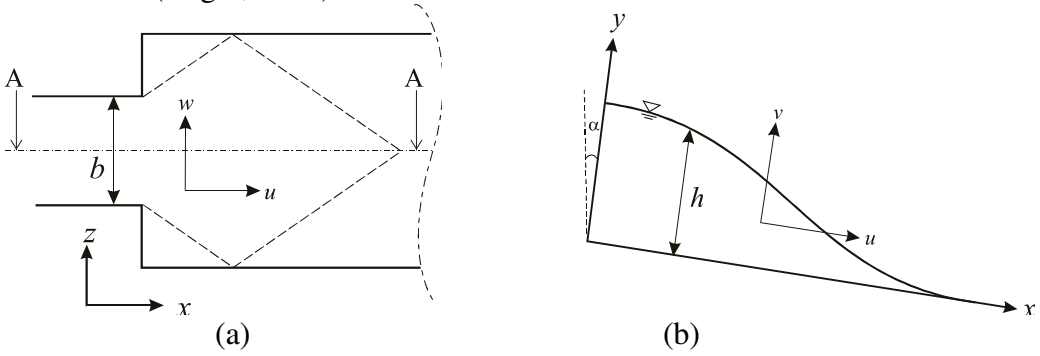

Fig. 2. (a) Abrupt expansion flow with *b* as width of the approach channel. (b) Schematic of section A-A

THEORETICAL ANALYSIS

The abrupt expansion flow in steady state shown in Figure 2(a) and Figure 2(b) can be represented by the following steady state depth-averaged equations;
Continuity equation:

$$\frac{\partial hu}{\partial x}+\frac{\partial hw}{\partial z}=0 \tag{1}$$

Momentum equation:

$$\begin{aligned}\frac{\partial hu^2}{\partial x}+\frac{\partial huw}{\partial z}&=-gh\frac{\partial h}{\partial x}+gh\sin\alpha-\frac{\tau_{bx}}{\rho}\\ \frac{\partial huw}{\partial x}+\frac{\partial hw^2}{\partial z}&=-gh\frac{\partial h}{\partial z}-\frac{\tau_{bz}}{\rho}\end{aligned} \tag{2}$$

where u and w are the depth-averaged velocity in x and z direction respectively, h is the flow depth, τ_{bx} and τ_{bz} are the bottom shear stress in x and z direction respectively, α is the slope of the channel and g is the gravity acceleration. Eq. 1 and Eq. 2 can be rearranged into matrix form as follows;

$$A_1\frac{\partial U}{\partial x}+A_2\frac{\partial U}{\partial z}=B \tag{3}$$

where U, A_1, A_2 and B are defined as,

$$\begin{aligned}u&=\begin{bmatrix}h\\u\\w\end{bmatrix}, & A_1&=\begin{bmatrix}u&h&0\\g&u&0\\0&0&u\end{bmatrix}\\ A_2&=\begin{bmatrix}w&0&h\\0&w&0\\g&0&w\end{bmatrix}, & B&=\begin{bmatrix}0\\g\sin\alpha-\tau_{bx}/(\rho h)\\ \tau_{bx}/(\rho h)\end{bmatrix}\end{aligned} \tag{4}$$

The Eigen values for A_1A_2 are λ_1, λ_2 and λ_3 which easily determined as follows;

$$\lambda_1=\frac{dz}{dx}=\frac{w}{u} \tag{5}$$

$$\lambda_1=\frac{dz}{dx}=\frac{uw+\sqrt{gh(u^2+w^2-gh)}}{u^2-gh} \tag{6}$$

$$\lambda_2=\frac{dz}{dx}=\frac{uw-\sqrt{gh(u^2+w^2-gh)}}{u^2-gh} \tag{7}$$

The corresponding Eigen vectors for λ_1, λ_2 and λ_3 are μ_1, μ_2 and μ_3, which are defined as follows;

For λ_1 $$\mu_1=\left[1,\ \frac{u}{g},\ \frac{w}{g}\right] \tag{8}$$

For λ_2 $$\mu_2=\left[\frac{\sqrt{gh(u^2+w^2-gh)}}{gh},\ -\frac{w}{u},\ 1\right] \tag{9}$$

For λ_3 $$\mu_3=\left[-\frac{\sqrt{gh(u^2+w^2-gh)}}{gh},\ -\frac{w}{u},\ 1\right] \tag{10}$$

From Eq. 5 we can see that the characteristic line λ_1 is a stream line. Eq. 6 and Eq. 7 indicate that the equations are hyperbolic if the flow is super-critical ($\sqrt{u^2+w^2}/gh$ is over unity). By multiplying the basic equations in Eq. 3 with the eigen vectors μ_1, μ_2 and μ_3 the equations that satisfy the characteristic lines are derived as follows;

With $i = 1,2,3$

$$\mu_i\left(\frac{\partial U}{\partial x} + A_1^{-1}A_2\frac{\partial U}{\partial z}\right) = \mu_i\left(\frac{\partial U}{\partial x} + \lambda_i\frac{\partial U}{\partial z}\right) = \mu_i A_1^{-1}B \tag{11}$$

or,

For i=1

$$\frac{\partial}{\partial x}\left(h + \frac{u^2+w^2}{2g}\right) + \frac{w}{u}\frac{\partial}{\partial x}\left(h + \frac{u^2+w^2}{2g}\right) = \sin\alpha - \frac{\tau_{bx}}{\rho g h} - \frac{\tau_{bz}}{\rho g h}\frac{w}{u} \tag{12}$$

For i=2

$$\begin{aligned}&\frac{\sqrt{gh(u^2+w^2)}}{hu}\left(\frac{\partial h}{\partial x} + \lambda_2\frac{\partial h}{\partial z}\right) - \frac{w}{u}\left(\frac{\partial u}{\partial x} + \lambda_2\frac{\partial u}{\partial z}\right) - \left(\frac{\partial w}{\partial x} + \lambda_2\frac{\partial w}{\partial z}\right)\\ &= \left(g\sin\alpha - \frac{\tau_{bx}}{\rho h}\right)\frac{uw + \sqrt{gh(u^2+w^2-gh)}}{u(gh-u^2)} - \frac{\tau_{bz}}{\rho h u}\end{aligned} \tag{13}$$

If the bottom shear stresses of the channel are neglected ($\tau_{bx} = \tau_{bz} = 0$) and the channel slope is zero ($\alpha = 0$), Eq. 12 and Eq. 13 can be reduced to following form,

From Eq. 12

$$\frac{V^2}{2g} + h = H_o = constant \tag{14}$$

From Eq. 13

$$\frac{1}{V}\frac{dV}{d\theta} = \frac{\sqrt{H_o - V^2/(2g)}}{\sqrt{3V^2/(2g) - H_o}} \tag{15}$$

where V and θ are defined as,

$$\begin{aligned}V &\equiv \sqrt{u^2+w^2}\\ \tan\theta &= w/u\end{aligned} \tag{16}$$

By introducing $V' = V/\sqrt{2gH_o}$, the dimensionless form of Eq. 14 and Eq. 15 can be written as follows,

$$V'^2 + \frac{h}{H_o} = 1 \tag{17}$$

$$\frac{1}{V'}\frac{dV'}{d\theta} = \frac{\sqrt{1-V'^2}}{\sqrt{3V'^2-1}} \tag{18}$$

By integrating Eq. 18, the solution for θ can be obtained as follows,

$$\theta = \sqrt{3}\ \tan^{-1}\sqrt{\frac{3h}{2H_o}\Big/\left(1-\frac{3h}{2H_o}\right)} - \tan^{-1}\left(\frac{1}{\sqrt{3}}\right)\cdot\sqrt{\frac{3h}{2H_o}\Big/\left(1-\frac{3h}{2H_o}\right)} - \theta_1 \tag{19}$$

with θ_1 is the integral constant defined by the condition that for $\theta = 0$, the initial depth is $h = h_1$. By using Eq. 17, the relation between Froude number, Fr and h/H_o can be defined as follows,

$$\frac{h}{H_o} = 1 - V'^2 = 1 - \frac{h}{H_o}\frac{1}{2}Fr^2 = \frac{2}{2+Fr^2} \tag{20}$$

The solution in Eq. 19 can therefore be expressed in Fr number as follows;

$$\theta = \sqrt{3}\, tan^{-1}\frac{\sqrt{3}}{\sqrt{Fr^2-1}} - tan^{-1}\frac{1}{\sqrt{Fr^2-1}} - \theta_1 \tag{21}$$

Ippen (1951) derived the same solution as in Eq. 19 and Eq. 21 by using different approach. It is worth to note that from Eq. 18 and Eq. 17, the solution in Eq. 19 and Eq. 21 are valid under the maximum and minimum conditions below;

$$V' = 1, \quad \theta = 0^o, \quad h/H_o = 0, \quad \therefore \text{From Eq. 20}, \quad Fr = \infty \tag{22}$$

$$V' = 1/\sqrt{3}, \quad \theta = 65^o 53', \quad h/H_o = 2/3, \quad \therefore \text{From Eq. 20}, \quad Fr = 1.0 \tag{23}$$

The flow near the abrupt expansion can be regarded as flow subjected to continuous disturbances. The angle of the disturbance wave (shock wave) β shown accompanied by the change of flow direction θ is shown in Figure 3. In the case where the depth difference across the shock wave is small, angle β is given in simplified form as follows (Ippen, 1951);

$$sin\,\beta = \frac{1}{Fr} \tag{24}$$

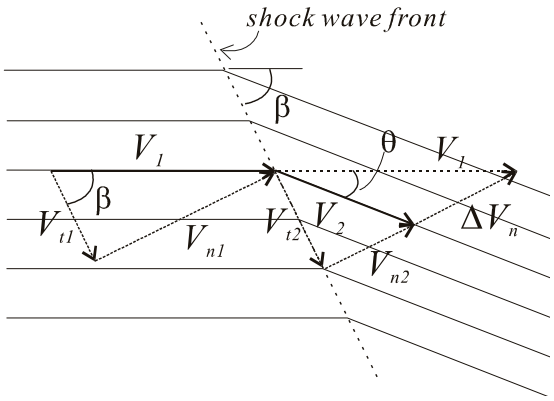

Figure 3. Flow with velocity V_1 (before flow direction change) and velocity V_2 (after flow direction change), with shock wave angle, β and angle of change in flow direction, θ

NUMERICAL MODEL

Governing Equations

A free-surface three-dimensional model based on the SOLA-VOF algorithm (Hirt and Nicholas, 1981) is used to simulate the abrupt expansion flow. The governing equations used in the numerical model are as follows;

Continuity equation,

$$\frac{\partial u}{\partial x} + \frac{\partial v}{\partial y} + \frac{\partial w}{\partial z} = 0 \tag{25}$$

Momentum equation,

$$\begin{aligned}
\frac{\partial u}{\partial t} + \frac{\partial u^2}{\partial x} + \frac{\partial uv}{\partial y} + \frac{\partial uw}{\partial z} &= g_x - \frac{\partial P}{\partial x} + \nu\nabla^2 u \\
\frac{\partial v}{\partial t} + \frac{\partial uv}{\partial x} + \frac{\partial v^2}{\partial y} + \frac{\partial vw}{\partial z} &= g_y - \frac{\partial P}{\partial y} + \nu\nabla^2 v \\
\frac{\partial w}{\partial t} + \frac{\partial uw}{\partial x} + \frac{\partial vw}{\partial y} + \frac{\partial w^2}{\partial z} &= g_z - \frac{\partial P}{\partial z} + \nu\nabla^2 w
\end{aligned} \tag{26}$$

SOR (Successive Over Relaxation) method is used in the pressure iteration where pressure is adjusted iteratively to satisfy the continuity equation based on the SOLA-VOF algorithm. The VOF density function F is advected in its conservative form as follows,

$$\frac{\partial F}{\partial t}+\frac{\partial uF}{\partial x}+\frac{\partial vF}{\partial y}+\frac{\partial wF}{\partial z}=0 \tag{27}$$

The CIP Scheme

The CIP method (Yabe, 1991) is a higher-order, less diffusive numerical scheme that solves the general hyperbolic equation as follows;

$$\frac{\partial \boldsymbol{f}}{\partial t}+(\boldsymbol{u}\cdot\nabla)\boldsymbol{f}=0 \tag{28}$$

In the presence of non-advection term $\boldsymbol{G}$, the hyperbolic equation in Eq. 28 becomes,

$$\frac{\partial \boldsymbol{f}}{\partial t}+(\boldsymbol{u}\cdot\nabla)\boldsymbol{f}=\boldsymbol{G} \tag{29}$$

In CIP method, the spatial gradient of $\boldsymbol{f}$ is also advected. Based on Eq. 29, the equation for the advection of spatial gradient $\partial_\alpha \boldsymbol{f}$ is as follows,

$$\frac{\partial(\partial_\alpha \boldsymbol{f})}{\partial t}+(\boldsymbol{u}\cdot\nabla)(\partial_\alpha \boldsymbol{f})=\boldsymbol{K} \tag{30}$$

with $\boldsymbol{K}=(\partial_\alpha \boldsymbol{G})-[(\partial_\alpha \boldsymbol{u})\cdot\nabla]f$ and α = *x,y or z* direction. In order to apply the CIP scheme to solve the hyperbolic equation with the presence of non-advection term as in Eq. 29 and Eq. 30, time-splitting technique is applied where the equation is solved in two phases: the advection phase and the non-advection phase (Yabe, 1991). The procedure is summarized as follows;

Solving non-advection phase:

$$\frac{\partial \boldsymbol{f}}{\partial t}=\boldsymbol{G} \tag{31}$$

$$\frac{\partial(\partial_\alpha f)}{\partial t}=\boldsymbol{K} \tag{32}$$

Based on Eq. 30 and Eq. 31 the quantity $\boldsymbol{f}$ and its gradient $\partial_\alpha \boldsymbol{f}$ are advanced as follows;

$$\boldsymbol{f}^{*}=\boldsymbol{f}^{n}+\boldsymbol{G}\Delta t \tag{33}$$

$$\partial_\alpha \boldsymbol{f}^{*}=\partial_\alpha \boldsymbol{f}^{n}+\frac{\delta_\alpha \boldsymbol{f}^{*}-\delta_\alpha \boldsymbol{f}^{n}}{\Delta t}-[(\delta_\alpha \boldsymbol{u})\cdot\nabla]\boldsymbol{f} \tag{34}$$

where δ_α and $[(\delta_\alpha \boldsymbol{u})\cdot\nabla]\boldsymbol{f}$ are defined as follows;

In α direction

$$\delta_\alpha f=\frac{f_{i+1}-f_{i-1}}{2\Delta\alpha} \tag{35}$$

$$[(\delta_\alpha \boldsymbol{u})\cdot\nabla]\boldsymbol{f}=\delta_\alpha u(\partial_x \boldsymbol{f})+\delta_\alpha v\big(\partial_y \boldsymbol{f}\big)+\delta_\alpha w(\partial_z \boldsymbol{f}) \tag{36}$$

The sign n means the value at time step n while the sign $*$ means the time after one time step in the non-advection phase.

Solving advection phase:

After the non-advection phase, the value of $\boldsymbol{f}^{*}$ and $\partial_\alpha \boldsymbol{f}^{*}$are advected using CIP scheme to obtain the value at the next time step $\boldsymbol{f}^{n+1}$ and $\partial_\alpha \boldsymbol{f}^{n+1}$.

The Navier-Stokes equation in Eq. 26 is solved based on the above procedure where,

$$\boldsymbol{f} = (u \quad v \quad w) \tag{37}$$

$$\boldsymbol{G} = \begin{pmatrix} g_x - \dfrac{\partial P}{\partial x} + \nu\nabla^2 u \\ g_y - \dfrac{\partial P}{\partial y} + \nu\nabla^2 v \\ g_z - \dfrac{\partial P}{\partial z} + \nu\nabla^2 w \end{pmatrix} \tag{38}$$

The $\boldsymbol{G}$ term in Eq. 37 containing the pressure and viscosity term is solved implicitly. For the advection of VOF density function F as in Eq. 27 using the CIP scheme, the $\boldsymbol{f}$ and $\boldsymbol{G}$ are defined as follows;

$$\boldsymbol{f} = (F) \tag{39}$$

$$\boldsymbol{G} = \left(-F\frac{\partial u}{\partial x} - F\frac{\partial v}{\partial y} - F\frac{\partial w}{\partial z}\right) \tag{40}$$

A digitizer of the following form is used in the advection of $\boldsymbol{F}$ using CIP scheme to avoid the smearing of function $\boldsymbol{F}$ which will contribute to the loss of sharp fluid interface (Yamada, 1998).

$$\phi(F) = tan[0.85\pi(F - 0.5)] \tag{41}$$

Numerical Simulation Set-up

Table 1. Numerical simulation conditions

Experiment number	FR2	FR4
Inflow Froude number, Fr	2.78	4.0
Boundary conditions	Non-slip	Slip
Kinematic viscosity, ν (m^2s^{-1})	1.0×10^{-6}	0.0
Approach depth, h_o (*mm*)	16	30
Approach width, b (*mm*)	100	100
Cell size, $\Delta x = \Delta y = \Delta z$ (*mm*)	2	5

The abrupt expansion flow is simulated numerically in a rectangular channel shown in Figure 2 in three dimensions. The dimension of the rectangular is 800mm in lateral *x*-direction, 200mm in transverse *y*-direction and 400mm in vertical *z*-direction. Continuous inflow boundary condition is set at the upstream of the channel and continuous outflow with zero pressure gradient is set at the downstream. Initial time step, $\Delta t = 0.00005\ s$ is used and adjusted to satisfy Courant ratio 0.25 during the simulation.

Two simulations with different conditions are carried out. The first simulation (**FR2**) is set up to simulate the condition in the laboratory experiment where the approach flow depth, h_o is set to *16mm* and approach velocity V_o is set based on *Fr=2.78* which is the condition in the laboratory experiment. The value of kinematic viscosity of water is used, $\nu = 1.0 \times 10^{-6} m^2 s^{-1}$. Non-slip condition is applied on all the boundary wall of the channel. In the

second simulation (**FR1**), inviscid fluid condition is used. *Fr=4.0* is used and h_o is increased to *30mm*. The simulations conditions of FR1 and FR2 are summarized in Table.1

LABORATORY EXPERIMENT

Laboratory experiment set-up consists of a Perspex channel set up in the condition shown in Figure 2 with lateral length of 4000mm, transverse width of 200mm and approach width *b* of 100mm. The slope of the channel is adjusted to obtain a desirable approach depth h_o and Froude number. When the flow achieves steady state condition, the depth of the flow is measured in the interval of 10mm from the upstream of the channel to the point where the shock waves reflected from the channel side walls meet again at the middle of the channel (which is at the end of the core flow).

RESULTS AND DISCUSSION

Laboratory Experiment Result

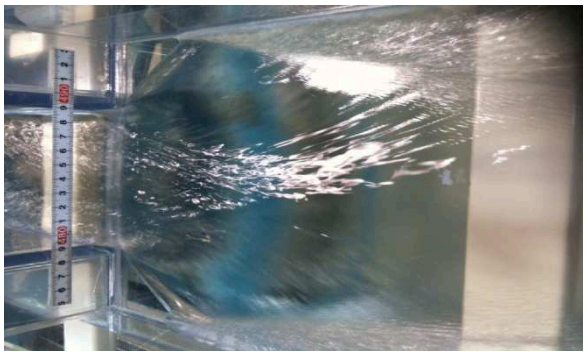

Fig.4. Laboratory experiments with Fr=2.78 and $h_o = 16mm$

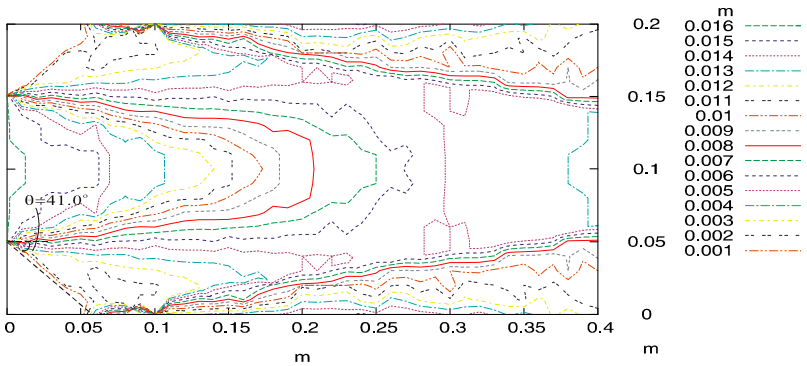

Fig. 5. Flow depth contour from laboratory experiment with Fr=2.78 and $h_o = 16mm$

Flow condition of FR2 in Table 1 is obtained in the laboratory experiment where the Fr=2.78 and approach depth $h_o = 16$mm. The flow in steady state is shown in Figure 4 while the depth-contour of the flow is plotted in Figure 5. The results shown in Figure 4 and Figure 5 clearly show the formation of core-flow, zero depth line as well as the shock waves. The flow spreads almost linearly near the expansion before impinging the boundary wall. Formation of shock wave propagating from the point of impingement to the center of the channel can be seen clearly as well. The zone of constant depth and velocity (zone ABC in Figure 1) is

however hard to detect in the laboratory experiment due to the size to the set-up and flow condition such as Froude number. Therefore the angle β is not measured for.

Numerical Simulation Result

The numerical simulation results are plotted in the form of depth-contour shown in Figure 6 and Figure 7. In the case of numerical simulation, the angle of zero depth line (or the change of flow direction) θ is determined by drawing a line connecting the point where the sudden expansion of flow starts at the inlet to the point of impingement at the boundary wall. This line is shown in Figure 1 as line CF. The value of θ can be determined analytically in Eq. 19 or Eq. 21. The value of β is determined by drawing a line connecting the upstream inlet where the sudden expansion of flow starts to the point at the center of the flow where the depth is equivalent to h_o which is shown in Figure 1 as line CB. Due to the limitation of the contour plot, the contour line nearest to the value of h_o is used to determine β.

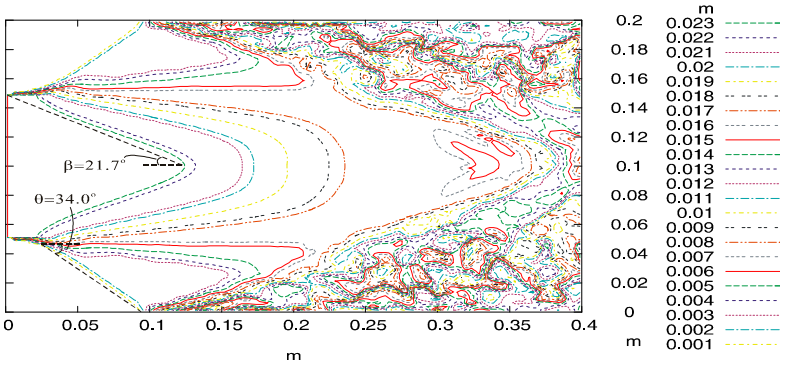

Fig. 6. Flow depth contour from numerical simulation with Fr=2.78 and $h_o = 16mm$

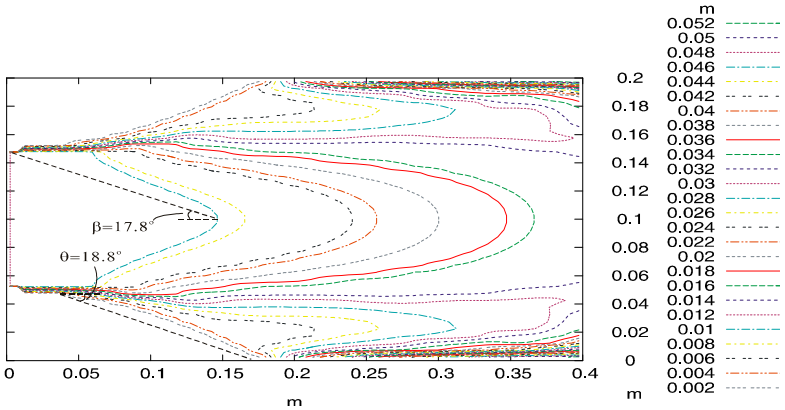

Fig. 7. Flow depth contour from numerical simulation with Fr=4.0 and $h_o = 30mm$

Discussion

The value θ and β from the laboratory experiment and numerical simulation results are compared with the analytical value obtained from Eq. 21 and summarized in Table 2. Based on Table 2, it can be seen that θ from laboratory experiment (41.0^o) is larger than the numerical (34.0^o) and analytical value (37.0^o). It is thought that this is due to the effect of bottom shear stress in the laboratory flow channel. Since the flow depth at the zero-depth line is shallow, the effect of adhesion is thought to contribute to larger θ value.

Table 2. Comparison of θ and β values

Angle in degree	FR2 (*Fr=2.78*)	FR4 (*Fr=4.0*)
θ from numerial simulation	34.0	18.8
θ from analytical	37.0	20.0
θ from laboratory experiment	41.0	-
β from numerial simulation	21.7	17.8
β from analytical	21.1	14.5
β from laboratory experiment	not measurable	-

In the case of $\boldsymbol{Fr = 2.78}$, both the values of $\boldsymbol{\theta}$ and $\boldsymbol{\beta}$ from the numerical model ($\boldsymbol{\theta = 34.0^o, \beta = 21.7^o}$) have good agreement with the analytical value ($\boldsymbol{\theta = 37.0^o, \beta = 21.1^o}$). In the case of $\boldsymbol{Fr = 4.0}$, the agreement of $\boldsymbol{\theta}$ value between the numerical model ($\boldsymbol{\theta = 18.8^o}$) and analytical value ($\boldsymbol{\theta = 20.0^o}$) is also good. The agreement of $\boldsymbol{\beta}$ value between the numerical model ($\boldsymbol{\beta = 17.8^o}$) and analytical value ($\boldsymbol{\beta = 14.5^o}$) is satisfactory. Therefore, it can be said that the numerical model could reproduce the angle of flow expansion $\boldsymbol{\theta}$ and angle of shock wave $\boldsymbol{\beta}$ with good accuracy. It is thought that the laboratory experiment result can be improved by using a larger set-up to reduce the effect contributed by the adhesion effect at the zero-depth line.

CONCLUSIONS

The abrupt expansion flow phenomenon is investigated qualitatively and quantitatively in this study. The formation of zero-depth line, core flow and shock waves are reproduced using numerical model. The performance of the numerical model is shown to be good as the values of flow expansion θ and shock wave angle β are in good agreement with the analytical values. However, more parameter such as the attenuation of flow along the center of the channel and the depth of flow at the channel wall after the impingement points are needed to further increase the reliability of the numerical model. The author plans to include the turbulence term in the model in the future.

REFERENCES

Hager, C.W. et al. 1992. Supercritical flow at abrupt expansion. *J. Compt. Phys.*, 39, 201-225.

Hosoda, T. and Yoneyama, N. 1994. Numerical analysis of high velocity flow with zero-depth line and oblique shock wave in steep open-channels. *Hydraulics Eng.*, 4, 1270-1274

Ippen, A.T. et al. 1951. High-velocity flow in open channels: A symposium. *Trans. ASCE*, 116 , 265-400.

Yabe, T. 1991. A universal cubic interpolation solver for compressible and incompressible fluids. *Shock Waves*, 1, 187-195.

Yamada, F., Takikawa, K., Iio, M., 1998. Computational accuracy of the VOF method using the CIP method for solving advections of density functions. *J. App. Mech. JSCE*, (in Japanese) 1, 283-292.